

# The XMM-Newton/2dF survey - II. The nature of X-ray faint optically bright X-ray sources.

A. Georgakakis<sup>1\*</sup>, I. Georgantopoulos<sup>1</sup>, M. Vallbé<sup>2</sup>, V. Kolokotronis<sup>1</sup>, S. Basilakos<sup>1</sup>, M. Plionis<sup>1,3</sup>, G. C. Stewart<sup>4</sup>, T. Shanks<sup>2</sup>, B. J. Boyle<sup>5</sup>

<sup>1</sup> *Institute of Astronomy & Astrophysics, National Observatory of Athens, I. Metaxa & V. Pavlou, Athens, 15236, Greece*

<sup>2</sup> *Physics Department, University of Durham, Science Labs, South Road, Durham, DH1 3LE, UK*

<sup>3</sup> *Instituto Nacional de Astrofísica, Óptica y Electrónica (INAOE), Apartado Postal 51 y 216, 72000, Puebla, Mexico*

<sup>4</sup> *Department of Physics and Astronomy, University of Leicester Leicester LE1 7RH, UK*

<sup>5</sup> *Anglo-Australian Observatory, PO Box 296, Epping, NSW 2121, Australia*

31 October 2018

## ABSTRACT

In this paper we investigate the properties of low X-ray-to-optical flux ratio sources detected in a wide area ( $2.5\text{deg}^2$ ) shallow [ $f_X(0.5 - 8\text{keV}) \approx 10^{-14}\text{erg s}^{-1}\text{cm}^{-2}$ ] XMM-Newton survey. We find a total of 26 sources (5% of the total X-ray selected population) with  $\log f_X/f_{opt} < -0.9$  to the above flux limit. Optical spectroscopy is available for 20 of these low X-ray-to-optical flux ratio objects. Most of them are found to be associated with Galactic stars (total of 8) and broad line AGNs (total of 8). We also find two sources with optical spectra showing absorption and/or narrow emission lines and X-ray/optical properties suggesting AGN activity. Another two sources are found to be associated with low redshift galaxies with narrow emission line optical spectra, X-ray luminosities  $L_X(0.5 - 8\text{keV}) \approx 10^{41}\text{erg s}^{-1}$  and  $\log f_X/f_{opt} \approx -2$  suggesting ‘normal’ star-forming galaxies. Despite the small number statistics the sky density of ‘normal’ X-ray selected star-forming galaxies at the flux limit of the present sample is low consistent with previous ROSAT HRI deep surveys. Also, the number density estimated here is in good agreement with both the  $\log N - \log S$  of ‘normal’ galaxies in the Chandra Deep Field North (extrapolated to bright fluxes) and model predictions based on the X-ray luminosity function of local star-forming galaxies.

**Key words:** Surveys – Galaxies: normal – X-rays: galaxies – X-rays: general

## 1 INTRODUCTION

X-ray surveys with the *ROSAT* and more recently with the *Chandra* and the XMM-Newton observatories have demonstrated that the X-ray source population is a heterogeneous mix of objects comprising (i) powerful AGNs/QSOs, (ii) galaxy groups/clusters, (iii) low luminosity AGNs, (iv) ‘normal’ galaxies with X-ray emission dominated by stellar processes and (v) a small number of Galactic stars (Lehmann et al. 2001; Barger et al. 2002; Hornschemeier et al. 2003).

Powerful AGNs are identified in X-ray surveys by their enhanced X-ray-to-optical flux ratios  $\log f_X/f_{opt} \gtrsim -1$ . These sources are responsible for the bulk of the diffuse X-Ray Background (XRB) and are therefore important for constraining models on the XRB origin.

In addition to powerful AGNs, deep surveys with the *Chandra* observatory reaching fluxes well below  $f(0.5 - 2\text{keV}) \lesssim 10^{-15}\text{erg s}^{-1}\text{cm}^{-2}$  have revealed large numbers of low X-ray-to-optical flux ratio sources  $\log f_X/f_{opt} \lesssim -1$ . These objects although too faint to significantly contribute to the XRB are detected in increasing numbers with decreasing flux and are likely to outnumber powerful AGNs below  $f(0.5 - 2\text{keV}) \approx 10^{-17}\text{erg s}^{-1}\text{cm}^{-2}$  (Hornschemeier et al. 2003). The low X-ray-to-optical flux ratio regime is thought to be populated by Low Luminosity AGNs (LLAGNs) and ‘normal’ galaxies (Hornschemeier et al. 2003). Indeed, sources with  $-2 \lesssim \log f_X/f_{opt} \lesssim -1$  exhibit enhanced activity attributed to either starbursts or LLAGNs (Alexander et al. 2002; Bauer et al. 2002; Hornschemeier et al. 2003; Georgakakis et al. 2003b). Even lower X-ray-to-optical flux ratios,  $\log f_X/f_{opt} \lesssim -2$ , are believed to be quiescent Milky Way type galaxies (Hornschemeier

\* email: age@astro.noa.gr

et al. 2002; Georgakakis et al. 2003a; Hornschemeier et al. 2003) although the presence of heavily obscured AGNs cannot be excluded.

Deep Chandra surveys have provided valuable information on the nature of low  $f_X/f_{opt}$  sources at fluxes  $f(0.5 - 2 \text{ keV}) \lesssim 10^{-17} - 10^{-16} \text{ erg s}^{-1} \text{ cm}^{-2}$ . These surveys are not however suitable for the study of low  $f_X/f_{opt}$  sources at brighter fluxes because of the *Chandra* small field-of-view ( $\approx 0.07 \text{ deg}^2$ ). Indeed, due to the low surface density of these sources at bright fluxes wide area surveys are required to compile large statistically complete samples to elucidate their nature.

The *ROSAT* satellite with a field-of-view of  $\approx 0.30 \text{ deg}^2$  per pointing has probed the bright flux regime [ $f(0.5 - 2 \text{ keV}) \approx 10^{-15} \text{ erg s}^{-1} \text{ cm}^{-2}$ ] but has identified only a small number of low X-ray-to-optical flux ratio sources (Griffiths et al. 1995; Griffiths et al. 1996; Georgantopoulos et al. 1996; Lehmann et al. 2001). This can be attributed to (i) the poor positional accuracy of ROSAT rendering the optical identification of X-ray sources difficult and (ii) its low sensitivity making wide area surveys to the limit  $f(0.5 - 2 \text{ keV}) \approx 10^{-15} \text{ erg s}^{-1} \text{ cm}^{-2}$  time consuming. The latter is particularly true due to the low surface density of  $f_X/f_{opt} \lesssim -1$  sources to the flux limit above requiring large surveyed regions to compile statistically complete samples. Moreover, the insensitivity of ROSAT to hard X-rays ( $> 2.5 \text{ keV}$ ) is a major drawback since heavily obscured AGNs (believed to populate the  $\log f_X/f_{opt} \lesssim -1$  regime) are expected to emit most of their X-ray energy output in this spectral band.

In this paper we employ a shallow (2-10 ks) wide area ( $\approx 2.5 \text{ deg}^2$ ) XMM-*Newton* survey to explore the nature of the  $\log f_X/f_{opt} \lesssim -1$  sources to the limit  $f(0.5 - 8 \text{ keV}) \approx 10^{-14} \text{ erg s}^{-1} \text{ cm}^{-2}$  similar to that probed by previous *ROSAT* surveys. Compared to *ROSAT*, XMM-*Newton* has the advantage of significantly higher sensitivity over a wide energy range (0.2-10 keV) and improved positional accuracy ( $\lesssim 3.5 \text{ arcsec}$ ; Hasinger et al. 2001; McHardy et al. 2003) facilitating the optical identification of X-ray sources. Our XMM-*Newton* observations (hereafter referred to as the XMM/2dF survey) cover an area of  $\approx 2.5 \text{ deg}^2$  much larger than any previous *ROSAT* surveys at the same flux limit. This is essential to compile a large sample of low X-ray-to-optical flux ratio sources to explore their nature and to constrain the relative fraction of the different X-ray populations. An advantage of the data presented here is that unlike deep Chandra samples (e.g. Brandt et al. 2001) limited by the small field-of-view, the XMM/2dF survey has sufficient areal coverage to probe the low- $z$  ( $z \lesssim 0.1$ ) universe. This is essential to explore the nature of the relatively nearby X-ray population and to provide a link between local ( $< 100 \text{ Mpc}$ ) and more distant samples.

Moreover, our XMM/2dF survey has the advantage of high quality follow-up optical spectroscopic and photometric observations. Apart from our own spectroscopic campaign the XMM/2dF overlaps with large scale spectroscopic programs: the Sloan Digital Sky Survey (SDSS), the 2dF Galaxy and QSO Redshift Surveys (2dFGRS and 2QZ respectively). These unprecedented spectroscopic databases are complemented by a homogeneous set of multi-waveband (*ugriz*) photometric data from the SDSS available for part of our XMM/2dF survey.

Section 2 presents the XMM/2dF survey, section 3 describes the reduction of the X-ray data while sections 4 and 5 detail the optical photometric and spectroscopic observations respectively. In section 6 we outline the optical identification method while section 7 presents the sample employed in this study. The results are discussed in section 8. Finally section 9 summarises our conclusions. Throughout this paper we adopt  $H_0 = 65 \text{ km s}^{-1} \text{ Mpc}^{-1}$ ,  $\Omega_M = 0.3$  and  $\Omega_\Lambda = 0.7$ .

## 2 THE XMM/2DF SURVEY

The North Galactic Pole F864 region [RA(J2000)=13<sup>h</sup>41<sup>m</sup>; Dec.(J2000)=00°00′] and the South Galactic Pole [SGP; RA(J2000)=00<sup>h</sup>57<sup>m</sup>, Dec.(J2000)=-28°00′] were surveyed by the XMM-*Newton* between May 2002 and February 2003 as part of the Guaranteed Time program. The observations consist of a total of 18 pointings split between the SGP (total of 5) and the F864 (total of 8) regions each with an exposure time of  $\approx 2 - 10 \text{ ks}$ . Part of this dataset was presented by Georgakakis et al. (2003a). In the present paper the Georgakakis et al. (2003a) observations are supplemented by a total of three additional pointings recently obtained by the XMM-*Newton* in the F864 region. These three fields suffered from elevated particle background or instrumental problems and were re-observed by the XMM-*Newton* between January and February 2003. The EPIC (European Photon Imaging Camera; Strüder et al. 2001; Turner et al. 2001) cameras were operated in full frame mode with the thin filter applied.

Both the F864 and SGP regions overlap with the 2dF Galaxy Redshift Survey (2dFGRS<sup>†</sup>; Colless et al. 2001) and the 2dF QSO Redshift Survey (2QZ<sup>‡</sup>; Croom et al. 2001). Both the 2dFGRS and 2QZ are large-scale spectroscopic campaigns that fully exploit the capabilities of the 2dF multi-fibre spectrograph on the 4 m Anglo-Australian Telescope (AAT). These on-going projects aim to obtain high quality spectra, redshifts and spectral classifications for 250 000  $bj < 19.4 \text{ mag}$  galaxies and 25 000 optically selected  $bj < 20.85 \text{ mag}$  QSOs.

In addition to 2dF spectroscopy, the F864 region overlaps with the Sloan Digital Sky Survey (York et al. 2000). The SDSS is an on-going imaging and spectroscopic survey that aims to cover about 10 000  $\text{deg}^2$  of the sky. Photometry is performed in 5 bands (*ugriz*; Fukugita et al. 1996; Stoughton et al. 2002) to the limiting magnitude  $g \approx 23 \text{ mag}$ , providing a uniform and homogeneous multi-color photometric catalogue. The SDSS spectroscopic observations will obtain spectra for over 1 million objects, including galaxies brighter than  $r = 17.7 \text{ mag}$ , luminous red galaxies to  $z \approx 0.45$  and colour selected QSOs (York et al. 2000; Stoughton et al. 2002).

Unlike the F864 area, the SGP region does not have complete and homogeneous CCD photometric coverage. In the absence of good quality photometry for this field we use photographic data from the APM survey calibrated to the

<sup>†</sup> <http://msowww.anu.edu.au/2dFGRS/>

<sup>‡</sup> <http://www.2dfquasar.org>

Johnson-Cousin  $B$ -band using CCD photometry available for a subregion of the SGP field.

### 3 X-RAY DATA

A full description of the X-ray data reduction and the generation of the PN and MOS event files is presented by Georgakakis et al. (2003a). To increase the signal-to-noise ratio and to reach fainter fluxes the PN and the MOS event files have been combined into a single event list using the MERGE task of SAS. Images have been extracted in the spectral bands 0.5-8 (total), 0.5-2 (soft) and 2-8 keV (hard) for both the merged and the individual PN and MOS event files. We use the more sensitive (higher S/N ratio) merged image for source extraction and flux estimation, while the individual PN and MOS images are used to calculate hardness ratios. This is because the interpretation of hardness ratios is simplified if the extracted count rates are from one detector only.

Source extraction is performed in the 0.5-8 keV merged image using the EWAVELET task of SAS with a detection threshold of  $5\sigma$ . The extracted sources for each field were visually inspected and spurious detections clearly associated with CCD gaps, hot pixels or lying close to the edge of the field of view were removed. The final catalogue comprises a total of 516 X-ray sources to the limit  $f_X(0.5 - 8 \text{ keV}) \approx 10^{-14} \text{ erg s}^{-1} \text{ cm}^{-2}$ . Source detection using the EWAVELET task of SAS with a detection threshold of  $5\sigma$  is also performed in the individual soft (0.5-2 keV) and hard (2-8 keV) band merged images. A total of 483 and 175 sources are detected in the individual 0.5-2 and 2-8 keV bands respectively to the  $5\sigma$  detection threshold.

Count rates in the merged (PN+MOS) images as well as the individual PN and MOS images are estimated within an 18 arcsec aperture. For the background estimation we use the background maps generated as a by-product of the EWAVELET task of SAS. A small fraction of sources lie close to masked regions (CCD gaps or hot pixels) on either the MOS or the PN detectors. This may introduce errors in the estimated source counts. To avoid this bias, the source count rates (and hence the hardness ratios and the flux) are estimated using the detector (MOS or PN) with no masked pixels in the vicinity of the source.

To convert count rates to flux the Energy Conversion Factors (ECF) of individual detectors are calculated assuming a power law spectrum with  $\Gamma = 1.7$  and Galactic absorption  $N_H = 2 \times 10^{20} \text{ cm}^{-2}$  appropriate for both the SGP and the F864 fields. The mean ECF for the mosaic of all three detectors is estimated by weighting the ECFs of individual detectors by the respective exposure time. For the encircled energy correction, accounting for the energy fraction outside the aperture within which source counts are accumulated, we adopt we adopt the calibration given by the XMM-Newton Calibration Documentation §.

§ [http://xmm.vilspa.esa.es/external/xmm\\_sw\\_cal/calib/documentation.shtml#XRT](http://xmm.vilspa.esa.es/external/xmm_sw_cal/calib/documentation.shtml#XRT)

### 4 OPTICAL PHOTOMETRIC DATA

The F864 region overlaps with the SDSS (York et al. 2000) Early Data Release (EDR; Stoughton et al. 2002; <http://www.sdss.org>). Multiwaveband photometric observations (*ugriz*-filters; Fukugita et al. 1996) are available to the limiting magnitude  $r \approx 23$  mag with the star-galaxy separation being reliable to  $r = 21$  mag. In the present study the colour transformations of Fukugita et al. (1996) are used to convert SDSS  $g$ -band magnitudes to the standard Johnson-Cousin  $B$ -band.

In the SGP region in the absence of homogeneous CCD photometry we use data from the APM survey. These are calibrated to the standard Johnson-Cousin  $B$ -band using CCD broad-band photometry available for one of our X-ray pointings, SGP-2 [RA(J2000)=00<sup>h</sup>57<sup>m</sup>00<sup>s</sup>, Dec.(J2000)=-27°36'00"].

Photometric observations of this field in the Sloan *gri* filters were carried out at the AAT in 2000 December 27 using the Wide Field Imager (WFI). The WFI was mounted at the prime focus of AAT giving a pixel size of  $0.225 \text{ arcsec pixel}^{-1}$  and a field of view of  $30 \times 30 \text{ arcmin}^2$ . The total integration times were 2400 s in all three bands split into four separate 600 s exposures. The observations were reduced following standard procedures using Starlink and IRAF tasks. Photometric calibration was performed using standard stars from Landolt (1992). These provide the instrumental zero point, the atmospheric extinction relation and the colour terms for the conversion from Sloan filters to the standard Johnson-Cousin system used by Landolt. The uncertainty in the zero point estimated using these standard stars is  $\pm 0.05$  mag in all three bands. Source extraction and photometry is performed using the SExtractor package (Bertin & Arnouts 1996). Total Kron magnitudes are measured in the  $g$  and  $r$  filters to estimate  $g - r$  colours and to transform  $g$ -band magnitudes into the standard Johnson-Cousin  $B$ -band using the colour transformations derived above. A detailed description of these observations including data reduction, source extraction and catalogue generation will be presented in a forthcoming paper (Vallb  et al. 2003, in preparation).

Optical sources (both stars and galaxies) within the XMM/2dF survey SGP region are selected from the APM scans of the UKST  $bj$  plates¶. The APM magnitudes are recalibrated to the Johnson-Cousin  $B$ -band using our CCD photometry.

Firstly, the APM and the CCD source catalogues are cross-correlated using a 2 arcsec matching radius to identify common objects. We find 843 overlapping sources of which 375 are galaxies and 468 are classified stars by APM. These sources are used to estimate the calibration curve,  $B = f(m_{bj})$ , giving standard Johnson-Cousin  $B$ -band magnitude as a function of uncalibrated APM magnitude  $m_{bj}$ . Since the APM magnitudes are not corrected for emulsion saturation the calibration curve is expected to be non-linear. Following Maddox et al. (1990) we approximate  $f(m_{bj})$  using 2nd and 3rd order polynomials for galaxies and stars respectively (on the basis of the APM classification). The polynomial fit residuals for both galaxies and stars follow a

¶ <http://www.ast.cam.ac.uk/~apmcat>

Gaussian distribution with an rms of  $\approx 0.2$  mag. This is the  $1\sigma$  uncertainty of the calibrated APM magnitudes.

## 5 OPTICAL SPECTROSCOPIC DATA

In addition to publicly available spectroscopic data from 2dFGRS, 2QZ and the SDSS spectroscopic surveys we have initiated our own follow-up spectroscopic campaign of the XMM/2dF sources. A detailed description of these observations will be presented in a forthcoming paper (Georgakakis et al. in preparation).

In brief, X-ray sources in the F864 region of the XMM/2dF survey with optical counterparts brighter than  $B = 22$  mag were selected for multi-fibre spectroscopy using 2dF at the prime focus of the AAT. The 2dF consists of two spectrographs and two  $1024 \times 1024$  thinned Tektronix CCDs each receiving 200 fibres. The fibres are  $\approx 2$  arcsec in diameter resulting in 2 pixel wide spectra on the detectors.

The data were obtained in service time mode during 2003 March 26. Due to poor weather conditions at the time of the observation the total exposure time was limited to 1 h split into two half hour integrations. The grating used was the 300B providing a dispersion of  $4.3 \text{ \AA pixel}^{-1}$  and a wavelength resolution of  $\approx 9 \text{ \AA}$  ( $\approx 2$  pixels FWHM) over the range 3700–7900 Å.

The data reduction was performed using the pipeline reduction package 2DFDR developed for the reduction of the 2dF data. Fibre flat fields were employed to determine the positions of the fibre spectra on each CCD frame and to flat-field the data. A CuArHe arc lamp exposure was then used for the wavelength calibration. Redshifts were determined by visual inspection of the resulting spectra. Flux calibration has not been performed. This is due to the difficulty in obtaining absolute flux calibration for the 2dF fibres which can differ substantially in their throughput. This also applies to the 2dFGRS data. Therefore when presenting optical spectra (see Figure 2) we plot raw counts as a function of wavelength.

## 6 OPTICAL IDENTIFICATION

To optically identify the sources detected in the XMM/2dF survey we follow the method described by Downes et al. (1986) to calculate the probability a given candidate is the true identification using Bayes' theorem: Consider an optically detected candidate with magnitude  $m$  at a distance  $r$  from the X-ray position. Given the surface density of objects brighter than  $m$ ,  $\Sigma(< m)$ , the expected number of candidates within  $r$  is

$$\mu = \pi r^2 \Sigma(< m). \quad (1)$$

Assuming that source positions are Poissonian, the probability of at least one object brighter than  $m$  within radius  $r$  is

$$P = 1 - \exp(-\mu), \quad (2)$$

which reduces to  $\mu$  for  $\mu \ll 1$ . In this case, the candidate is unlikely to be a chance association. In the present study we apply an upper limit in the search radius,  $r < 7$  arcsec

and a cutoff in the probability,  $P < 0.05$ , to limit the optical identifications to those candidates that are least likely to be spurious alignments. The background density of sources (both galaxies and stars) in the Johnson-Cousin  $B$ -band is estimated using the SDSS  $g$ -band converted to the  $B$ -band using the transformations of Fukugita et al. (1996). At magnitudes fainter than  $B = 22.5$  mag where SDSS is affected by incompleteness we use the  $B$ -band surface density of Metcalfe et al. (1995). In the F864 region for the optical identification we only consider SDSS sources brighter than  $B = 22.5$  mag to avoid the SDSS incompleteness at fainter magnitudes. Similarly, in the SGP region we only consider APM sources brighter than  $B = 21.5$  mag.

We propose 164 candidate optical identifications out of 291 0.5–8 keV selected sources in the F864 region and 57 identifications out of 223 X-ray sources in the SGP region.

The probability  $P$  above is estimated under the assumption that the source positions follow the Poisson distribution. To assess the fraction of spurious optical identifications using the real spatial distribution of sources we perform Monte Carlo simulations. Mock X-ray catalogues are constructed by randomising the positions of the X-ray sources within the area covered by the XMM-Newton observations. The optical identification method is performed on the mock catalogues using the same criteria ( $P < 0.05$ ,  $\delta r < 7$  arcsec,  $B < 21.5$  or  $B < 22.5$  mag) as for the real sources. This procedure is repeated 100 times. We find a spurious rate of  $\approx 6\%$  slightly larger than the probability cutoff,  $P$ , assuming Poisson distribution for the source positions.

## 7 THE SAMPLE

The sample used in the present study is compiled from the  $5\sigma$  threshold 0.5–8 keV source catalogue by identifying and selecting low X-ray-to-optical flux ratio sources,  $\log f_X/f_{opt} < -0.9$ . The X-ray-to-optical flux ratio is estimated from the 0.5–8 keV flux  $f(0.5-8 \text{ keV})$  and the  $B$ -band magnitude according to the relation

$$\log \frac{f_X}{f_{opt}} = \log f(0.5 - 8 \text{ keV}) + 0.4 B + 4.89. \quad (3)$$

The equation above is derived from the X-ray-to-optical flux ratio definition of Stocke et al. (1991) that involved 0.3–3.5 keV flux and  $V$ -band magnitude. These quantities are converted to 0.5–8 keV flux and  $B$ -band magnitude assuming a mean colour  $B - V = 0.8$  and a power-law X-ray spectral energy distribution with index  $\Gamma = 1.7$ .

The 0.5–8 keV selected sample with  $\log f_X/f_{opt} < -0.9$  is presented in Table 1 which has the following format:

1. Name of the most probable optical counterpart of the X-ray source. If a name is not available we use the prefix ‘‘XMM2DF’’ followed by the RA and DEC coordinates of the X-ray source in J2000.

2-3. Right ascension ( $\alpha_X$ ) and declination ( $\delta_X$ ) of the X-ray source position in J2000.

4. Offset in arcseconds between the X-ray source centroid estimated by the EWAVELET task of SAS and the optical source centre. We note that the X-ray source centroid does not always coincide with the peak of the X-ray emission.

5. Optical  $B$ -band magnitude.

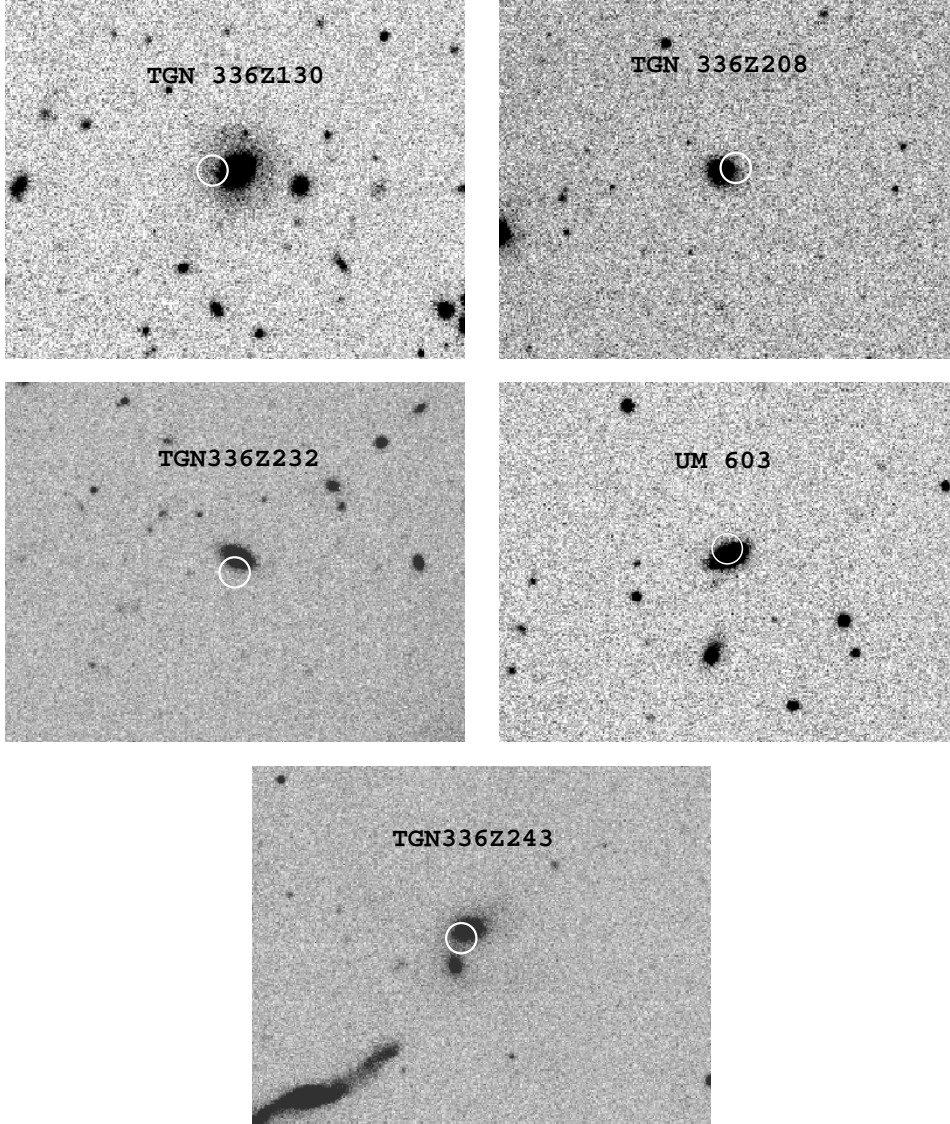


**Figure 1.** Optical (*r*-band) images of the low X-ray-to-optical flux ratio sources identified with low redshift galaxies ( $z < 0.1$ ). These sources include the two ‘normal’ galaxy candidates (TGN 336Z243, UM 603) and the three systems likely to host LLAGNs (TGN 336Z130, TGN 336Z208, TGN 336Z232) of which one shows broad emission line optical spectrum. The optical spectra of these systems are shown in Figure 2. The position of the X-ray centroid estimated by the EWAVELET task is overlaid on the optical image. The white circles have radius of 4 arcsec.

**6.** Optical morphology of the source: 3 is for extended optical light profile (i.e. galaxy) and 6 is for unresolved optical light profile (i.e. star or QSO). The optical morphology classification is from the SDSS and the APM for sources in the F864 and SGP regions respectively.

**7.** Redshift. The source from which the redshift estimate was obtained is also listed in Table 1.

**8.** Spectral classification of the optical counterpart. Spectral classifications are obtained from the same source as the redshifts listed in the previous column.

**9.** Comments on the observed optical spectral features: **A:** absorption lines; **NL:** narrow emission lines; **BL:** broad emission lines; **EA:** both absorption and emission lines. If the most probable counterpart is a star we give its spectral type.

Table 2 presents the X-ray properties of the low  $\log f_X/f_{opt}$  sample. We list:

**1.** 0.5-2 and 2-8 keV count rates. Sources that are not detected in the 0.5-2 or 2-8 keV spectral bands above the  $5\sigma$  threshold are assigned an upper limit ( $3\sigma$ ) assuming Poisson statistics. A small number of sources are only detected in the 0.5-8 keV band but not in the individual 0.5-2 and 2-8 keV bands. For these sources an upper limit is estimated to both their 0.5-2 and 2-8 keV count rates.

**2.** 0.5-8 keV X-ray flux in  $\text{erg s}^{-1} \text{cm}^{-2}$ .

**3.** 0.5-8 keV X-ray luminosity in  $\text{erg s}^{-1}$ , if a redshift is available.

**4.** Hardness ratio, HR, defined

$$\text{HR} = \frac{\text{RATE}(2080) - \text{RATE}(0520)}{\text{RATE}(2080) + \text{RATE}(0520)}, \quad (4)$$

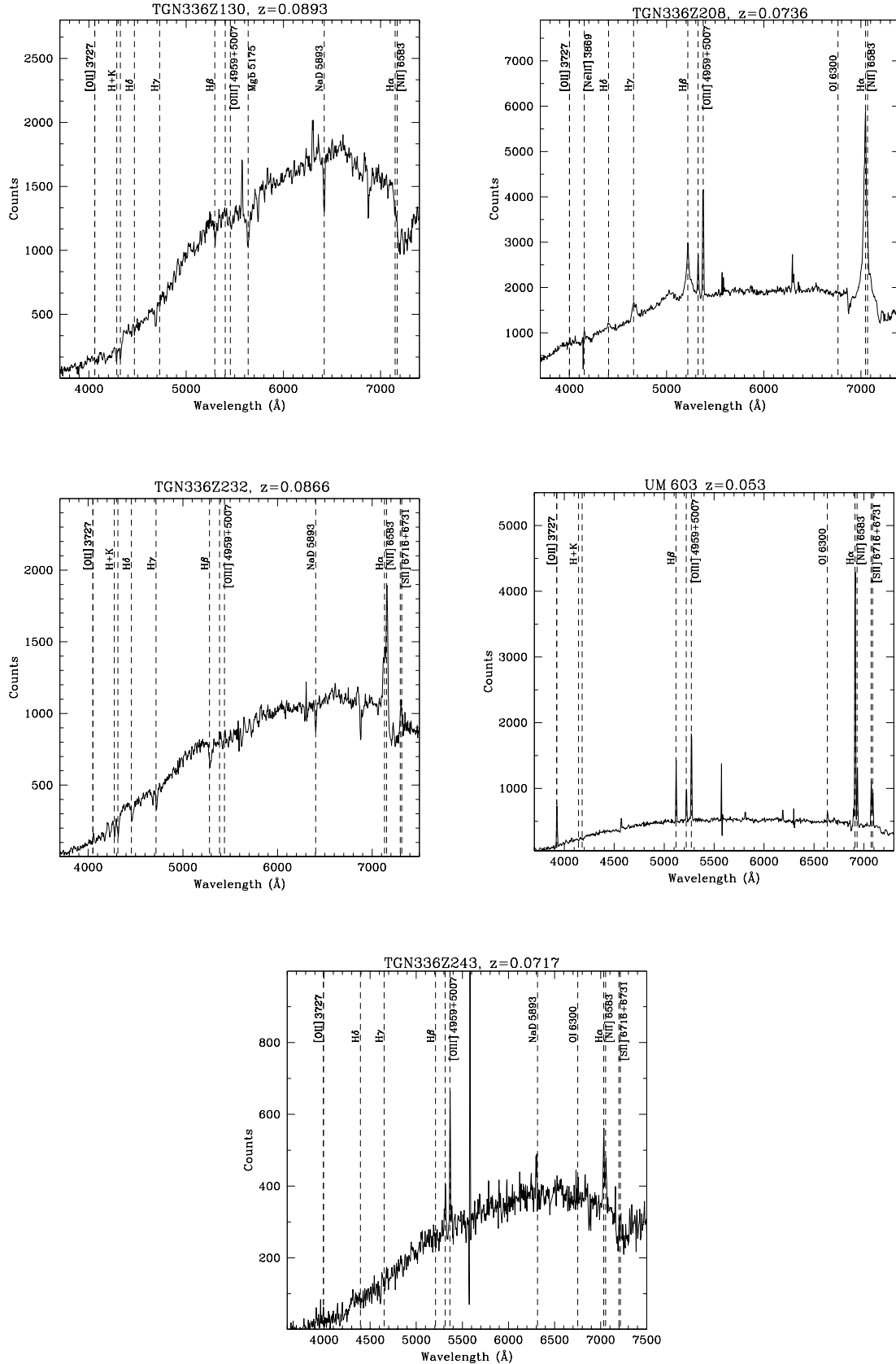


**Figure 2.** Optical spectra of the low X-ray-to-optical flux ratio sources identified with low- $z$  galaxies ( $z < 0.1$ ). These sources include the two ‘normal’ galaxy candidates (TGN 336Z243, UM 603) exhibiting narrow emission lines and the three systems likely to host LLAGNs (TGN 336Z130, TGN 336Z208, TGN 336Z232). The latter class comprises one galaxy with broad emission line optical spectrum while the remaining two show either absorption lines only or both absorption and weak narrow emission lines.

ID	NAME	$\alpha_X$ (J2000)	$\delta_X$ (J2000)	Offset (arcsec)	$B$ (mag)	Morphological type	$z$	Class	Comments <sup>a</sup>
1	SDSS J134521.45-000121.04	13 45 21.42	-00 01 22.5	1.6	16.99	6	0.0 <sup>1</sup>	star	M-type
2	TGN 336Z130	13 45 15.31	+00 15 15.9	6.7	17.63	3	0.0893 <sup>2</sup>	E/S0	A
3	SDSS J134514.98-000047.91	13 45 14.98	-00 00 47.6	0.4	13.69	6	-	-	-
4	SDSS J134501.7-002401.74	13 45 01.68	-00 24 02.5	0.9	18.24	6	0.0 <sup>1</sup>	star	F/G-type
5	SDSS J134433.57-000536.9	13 44 33.81	-00 05 37.0	3.5	19.97	6	0.0 <sup>3</sup>	star	M-type
6	2QZ J134427.9-003029	13 44 27.98	-00 30 32.3	3.7	19.44	6	1.374 <sup>1,4</sup>	QSO	BL
7	SDSS J134425.94-000056.2	13 44 25.97	-00 00 55.3	0.9	18.95	6	1.097 <sup>5</sup>	QSO	BL
8	TGN 336Z208	13 43 51.13	+00 04 38.8	3.4	17.62	3	0.0736 <sup>2</sup>	Scd	BL
9	2QZ J134314.8+002528	13 43 14.85	+00 25 29.3	0.4	19.78	6	1.468 <sup>4</sup>	QSO	BL
10	2QZ J134301.5-002951	13 43 01.57	-00 29 51.4	0.8	20.17	6	2.062 <sup>1,4</sup>	QSO	BL
11	SDSS J134235.91+002806.16	13 42 35.91	+00 28 10.0	3.9	13.81	6	0.0 <sup>1</sup>	star	F/G-type
12	SDSS J134232.84-002008	13 42 33.21	-00 20 05.7	6.0	17.48	6	-	-	-
13	SDSS J134228.98+001947.5	13 42 29.08	+00 19 44.7	3.1	14.28	6	0.0 <sup>1</sup>	star	G-type
14	TGN 336Z232	13 42 12.03	-00 17 37.4	2.8	17.65	3	0.0866 <sup>2</sup>	Sa	EA
15	UM 603	13 41 37.85	-00 25 55.3	2.4	16.86	3	0.053 <sup>1,6</sup>	H II	NL
16	2QZ J134133.6-00270	13 41 33.82	-00 27 02.8	2.5	19.84	6	1.341 <sup>4</sup>	QSO	BL
17	TGN 336Z243	13 41 33.22	-00 24 34.2	3.1	17.63	3	0.0717 <sup>2</sup>	Sa	NL
18	SDSS J134125.7-002208.06	13 41 25.69	-00 22 07.8	0.4	20.05	6	0.0 <sup>1</sup>	star	M-type
19	SDSS J134056.52+003156.29	13 40 56.52	+00 31 57.9	1.6	14.02	6	0.0 <sup>1</sup>	star	K-type
20	XMM2DF J005929.63-275316.07	00 59 29.63	-27 53 16.1	2.6	17.1	6	-	-	-
21	B005615.26-275548.8	00 58 40.48	-27 39 41.6	5.3	20.1	3	-	-	-
22	XMM2DF J005822.88-274014.03	00 58 22.88	-27 40 14.0	1.1	15.2	6	0.0 <sup>3</sup>	star	F/G-type
23	XMM2DF J005803.14-280856.05	00 58 03.14	-28 08 56.1	1.5	15.1	6	-	-	-
24	2QZ J005734.9-272828	00 57 34.92	-27 28 29.1	1.3	19.0	6	2.189 <sup>4</sup>	QSO	BL
25	2QZ J005701.1-272800	00 57 01.04	-27 28 01.6	2.2	19.7	6	0.825 <sup>4</sup>	QSO	BL
26	XMM2DF J005637.45-272717.47	00 56 37.45	-27 27 17.5	1.7	15.3	6	-	-	-

<sup>a</sup>A: absorption lines; NL: Narrow emission lines; BL: Broad emission lines; EA: absorption+emission lines

1: XMM/2dF spectroscopic program; 2: 2dFGRS; 3: Griffiths et al. (1995); 4: 2QZ; 5: SDSS; 6: Terlevich et al. (1991)

**Table 1.** Low X-ray-to-optical flux ratio sources in the XMM/2dF survey.

where RATE(0520) and RATE(2080) are the count rates in the 0.5-2 and 2-8 keV spectral bands respectively. Upper and lower limits are for sources that are not detected in the hard and soft bands respectively to the EWAVELET detection threshold of  $5\sigma$ . In the case of soft/hard band non-detection a  $3\sigma$  upper limit is estimated assuming Poisson statistics.

We note that for all the X-ray sources presented here the probability of an individual optical counterpart being spurious coincidence is small  $P \lesssim 6 \times 10^{-3}$ . Figure 1 shows the optical images of the low- $z$  sources ( $z < 0.1$ ) with the position of the X-ray centroid (estimated by the EWAVELET task) overlaid. The optical spectra of the same sources are presented in Figure 2.

Figure 3 plots  $B$ -band magnitude against 0.5-8 keV X-ray flux for both low  $f_X/f_{opt}$  sources and the whole X-ray selected sample. The  $\log(f_X/f_{opt}) = \pm 1$  lines in this figure delineate the region of the parameter space occupied by AGNs. Figure 4 plots the hardness ratio against X-ray-to-optical flux ratio for the low X-ray-to-optical flux ratio sources.

Notes on individual selected sources are presented in Appendix A. The classification of the present sample into different classes is performed on the basis of their optical spectroscopic (i.e. spectral features), photometric (i.e. resolved or point-like sources) and X-ray properties (i.e. X-ray luminosity, X-ray-to-optical flux ratio, HR). More information about the source classification can be found in Appendix A. The present sample of low X-ray-to-optical flux ratio sources to the limit  $f(0.5-8 \text{ keV}) \approx 10^{-14} \text{ erg s}^{-1} \text{ cm}^{-2}$

comprises: (i) 8 spectroscopically confirmed Galactic stars, (ii) 7 broad-line QSO, (iii) 3 LLAGNs of which one exhibits broad lines (TGN 336Z208) while the other two show absorption and/or narrow emission lines (TGN 336Z130, TGN 336Z232), (iv) 2 ‘normal’ galaxy candidates (UM 603, TGN 336Z243) and (v) 6 unclassified sources with no optical spectroscopic information. Most of the objects in the latter class are likely to be Galactic stars on the basis of their optical and X-ray properties.

We note that by LLAGN (e.g. class (iii) above) we refer to sources that show evidence for AGN activity and have X-ray luminosity  $L_X \lesssim 10^{42} \text{ erg s}^{-1}$  (e.g. Elvis, Soltan & Keel 1984). Indeed, the X-ray sources classified LLAGNs in our sample are nearby galaxies ( $z \lesssim 0.1$ ) with X-ray luminosities  $L(0.5-8 \text{ keV}) \approx 10^{42} \text{ erg s}^{-1}$  lower than those of distant QSOs. Two out of three (TGN 336Z130, TGN 336Z232) have  $\log f_X/f_{opt} \approx -1.5$  and optical spectra exhibiting both absorption and narrow emission lines.

The candidate ‘normal’ galaxies in the present sample have  $L(0.5-8 \text{ keV}) \approx 10^{41} \text{ erg s}^{-1}$ ,  $\log f_X/f_{opt} \approx -2$  and narrow emission line optical spectra. These values are elevated compared to quiescent spirals ( $L(0.5-8 \text{ keV}) \approx 10^{40} \text{ erg s}^{-1}$ ,  $\log f_X/f_{opt} \approx -3$ ; Hornschemeier et al. 2002; Georgakakis et al. 2003a; Hornschemeier et al. 2003) and typical to those of actively star-forming galaxies (e.g. Moran, Lehnert & Helfand 1999; Alexander et al. 2002; Bauer et al. 2002; Georgakakis et al. 2003b). We note that although the X-ray and optical properties of ‘normal’ galaxy candidates

ID	count rate <sup>a</sup> ( $\times 10^{-3}$ cnts s <sup>-1</sup> )		$f_X(0.5 - 8 \text{ keV})^b$ ( $\times 10^{-14}$ erg s <sup>-1</sup> cm <sup>-2</sup> )	$\log f_X/f_{opt}$	$L_X(0.5 - 8 \text{ keV})^b$ (erg s <sup>-1</sup> )	HR <sup>a</sup>
	0.5-2 keV	2-8 keV				
1	43.90 ± 8.84	< 13.8	12.4 ± 1.74	-1.22	-	< -0.52
2 <sup>c,*</sup>	3.13 ± 0.93	< 3.50	3.68 ± 1.02	-1.50	(8.38 ± 2.32) × 10 <sup>41</sup>	< 0.05
3	160.00 ± 12.80	7.97 ± 3.86	48.49 ± 2.65	-1.95	-	-0.91 ± 0.11
4	6.21 ± 2.03	5.53 ± 1.94	3.91 ± 0.56	-1.22	-	-0.06 ± 0.24
5	2.13 ± 2.14	< 8.69	1.03 ± 0.77	-1.11	-	< 0.61
6	< 7.77	< 6.57	0.82 ± 0.41	-1.42	(8.53 ± 4.26) × 10 <sup>43</sup>	-
7	11.00 ± 2.95	< 10.30	3.05 ± 0.57	-1.05	(1.89 ± 0.36) × 10 <sup>44</sup>	< -0.03
8 <sup>c,*</sup>	10.30 ± 1.59	3.34 ± 0.98	12.00 ± 1.61	-0.99	(1.81 ± 0.24) × 10 <sup>42</sup>	-0.51 ± 0.15
9 <sup>c</sup>	1.27 ± 0.51	< 1.37	1.29 ± 0.51	-1.09	(1.55 ± 0.62) × 10 <sup>44</sup>	< 0.04
10	3.55 ± 2.74	< 13.3	0.91 ± 0.73	-1.09	(2.38 ± 1.91) × 10 <sup>44</sup>	< 0.58
11	4.98 ± 2.37	< 6.05	2.39 ± 0.62	-3.21	-	< 0.10
12	0.84 ± 3.17	< 22.00	3.11 ± 0.88	-1.62	-	< 0.93
13	13.60 ± 3.86	< 7.44	3.88 ± 0.85	-2.81	-	< -0.29
14 <sup>*</sup>	6.06 ± 3.70	< 15.69	3.64 ± 1.08	-1.49	(7.82 ± 2.32) × 10 <sup>41</sup>	< 0.44
15	8.47 ± 2.46	< 6.32	1.95 ± 0.52	-2.08	(1.52 ± 0.40) × 10 <sup>41</sup>	< -0.15
16	2.93 ± 1.84	1.56 ± 1.50	1.52 ± 0.48	-0.99	(1.49 ± 0.48) × 10 <sup>44</sup>	-0.31 ± 0.55
17	< 9.76	< 5.42	1.31 ± 0.43	-1.95	(1.89 ± 0.63) × 10 <sup>41</sup>	-
18	3.96 ± 1.78	< 3.77	0.84 ± 0.39	-1.17	-	< -0.03
19	132.00 ± 8.25	3.51 ± 1.93	37.20 ± 1.64	-1.94	-	-0.95 ± 0.09
20	7.49 ± 2.18	< 5.26	1.99 ± 0.50	-1.99	-	< -0.18
21	1.66 ± 1.50	< 3.89	0.34 ± 0.35	-1.55	-	< 0.40
22	68.70 ± 7.06	-0.96 ± 1.29	22.50 ± 1.47	-1.69	-	-1.03 ± 0.15
23	105.00 ± 8.30	16.40 ± 3.82	42.30 ± 2.24	-1.43	-	-0.73 ± 0.09
24	6.70 ± 2.61	< 7.80	2.87 ± 0.65	-1.06	(8.53 ± 1.94) × 10 <sup>44</sup>	< 0.08
25	< 6.35	4.08 ± 2.06	1.88 ± 0.51	-0.98	(6.01 ± 1.66) × 10 <sup>43</sup>	> -0.22
26	24.00 ± 4.20	6.55 ± 2.68	10.20 ± 1.05	-2.00	-	-0.57 ± 0.18

<sup>a</sup>Count rates and hardness ratios are from EPIC-PN unless explicitly stated otherwise.

We define HR = (H - S)/(H + S) as in equation 4.

<sup>b</sup>Fluxes and luminosity estimates are from the merged images unless explicitly stated otherwise

<sup>c</sup>Count rates, hardness ratios and X-ray fluxes are from MOS

<sup>\*</sup>Classified LLAGN:  $L_X \lesssim 10^{42}$  erg s<sup>-1</sup> and optical/X-ray properties suggesting AGN activity

**Table 2.** X-ray properties of low X-ray-to-optical flux ratio sources in the XMM/2dF survey

are consistent with stellar origin for the X-ray emission we cannot exclude the possibility of LLAGN.

## 8 DISCUSSION

In the present study we use the wide area XMM/2dF survey to study low X-ray-to-optical flux ratio sources ( $\log f_X/f_{opt} < -0.9$ ) to the survey limit  $f(0.5 - 8 \text{ keV}) \approx 10^{-14}$  erg s<sup>-1</sup> cm<sup>-2</sup>. This translates to a soft band flux of  $f(0.5 - 2 \text{ keV}) \approx 5 \times 10^{-15}$  erg s<sup>-1</sup> cm<sup>-2</sup> (assuming  $\Gamma = 1.7$ ) comparable to previous *ROSAT* PSPC surveys. Out of 26 sources with  $\log f_X/f_{opt} < -0.9$  we find: (i) 8 spectroscopically confirmed Galactic stars, (ii) 7 broad-line QSO, (iii) 3 LLAGNs (for a definition of LLAGN class see section 7) of which one shows broad optical lines and the other two have absorption and/or narrow emission lines, (iv) 2 ‘normal’ galaxy candidates and (v) 6 unclassified sources with no optical spectroscopic information most of which are likely to be Galactic stars. The dominant populations to the flux limit of the present survey are Galactic stars and broad line QSOs with only a small fraction of LLAGNs and ‘normal’ galaxy candidates. The relatively mix of the low X-ray-to-optical flux ratio population found here is in fair agreement with the *ROSAT* HRI results of Lehmann et al. (2001) with the exception of the larger fraction of galaxy

groups identified by these authors. However, all the galaxy groups in the Lehmann et al. (2001) sample have fluxes  $f_X(0.5 - 2 \text{ keV}) < 5 \times 10^{-15}$  erg s<sup>-1</sup> cm<sup>-2</sup>, i.e. below the sensitivity limit of the present survey.

An interesting result from the present study is the identification of two ‘normal’ galaxy candidates. Recent deep *Chandra* surveys demonstrated beyond any doubt the appearance of ‘normal’ galaxies at faint X-ray fluxes ( $\lesssim 10^{-16}$  erg s<sup>-1</sup> cm<sup>-2</sup>; Hornschemeier et al. 2002; Bauer et al. 2002). Hornschemeier et al. (2003) used the 2Ms CDF-N survey to compile the first large X-ray selected sample of distant (median redshift  $\approx 0.3$ ) quiescent galaxies with  $\log f_X/f_{opt} \lesssim -2.3$ . They demonstrated that these systems comprise a non-negligible fraction ( $\approx 15\%$ ) of the X-ray population at  $f(0.5 - 2 \text{ keV}) \approx 2 \times 10^{-17}$  erg s<sup>-1</sup> cm<sup>-2</sup> and that their  $\log N - \log S$  rises much steeper than the general X-ray source population. The majority of the spectroscopically identified sources in the Hornschemeier et al. (2003) sample are emission-line galaxies most likely to be star-forming spirals in the redshift range  $0.06 \lesssim z \lesssim 0.85$ .

Our shallow wide area XMM/2dF survey complements the Hornschemeier et al. (2003) study by constraining the ‘normal’ galaxy  $\log N - \log S$  at much brighter fluxes  $f(0.5 - 8 \text{ keV}) \approx 10^{-14}$  erg s<sup>-1</sup> cm<sup>-2</sup>, albeit with poorer statistics. Figure 5 plots the cumulative ‘normal’ galaxy counts from



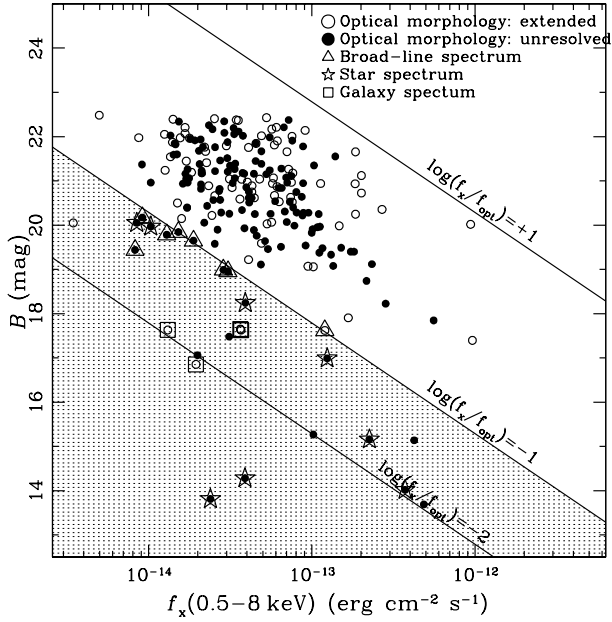


**Figure 3.**  $B$ -band magnitude against 0.5-8 keV flux. The  $\log f_X/f_{opt} < -1$  region studied here is shaded. Open circles are 0.5-8 keV X-ray detections with extended optical light profile. Filled circles are 0.5-8 keV X-ray detections with stellar-like optical light profile. A triangle on top of a symbol indicates broad line optical spectrum. A square on top of a symbol is for sources with optical spectra dominated by light from the host galaxy (e.g. narrow-emission and/or absorption lines). A star around a symbol indicates sources with Galactic star optical spectra. The lines indicate constant X-ray-to-optical flux ratios of +1, -1 and -2. The lines  $\log f_X/f_{opt} = \pm 1$  delineate the region of the parameter space occupied by powerful AGNs. The X-ray-to-optical flux ratio is defined in section 7.

the present sample (i.e. the two ‘normal’ galaxies identified here) and the CDF-N survey (Hornschemeier et al. 2003). Clearly, our surface density constraints suffer from small number statistics (e.g. only two ‘normal’ galaxy candidates). We note however, that the XMM/2dF survey with its wide field of view provides the only constraints to date to the surface density of the rare X-ray selected ‘normal’ galaxies at the flux limit of  $\approx 10^{-14}$  erg s $^{-1}$  cm $^{-2}$ .

Extrapolating the Hornschemeier et al. (2003) results to brighter flux limits using the best fit power-law they adopt to describe their  $\log N - \log S$  we find that our source counts are higher by a factor of  $\approx 5$ . However, taking into account the uncertainties in both our sample and that of Hornschemeier et al. (2003) there is agreement between the two studies. Also, we note that Hornschemeier et al. (2003) select only sources with  $\log f_X/f_{opt} \lesssim -2.3$ , i.e. quiescent low star-formation systems. This conservative selection threshold was chosen to avoid LLAGN contamination but is also likely to miss actively star-forming galaxies expected to have  $-1 \lesssim \log f_X/f_{opt} \lesssim -2$  (Alexander et al. 2002; Bauer et al. 2002).

Also shown in Figure 5 are the constraints from the stacking analysis results of Georgakakis et al. (2003a). These authors used the XMM/2dF survey to estimate the mean X-ray properties of optically selected 2dFGRS spi-

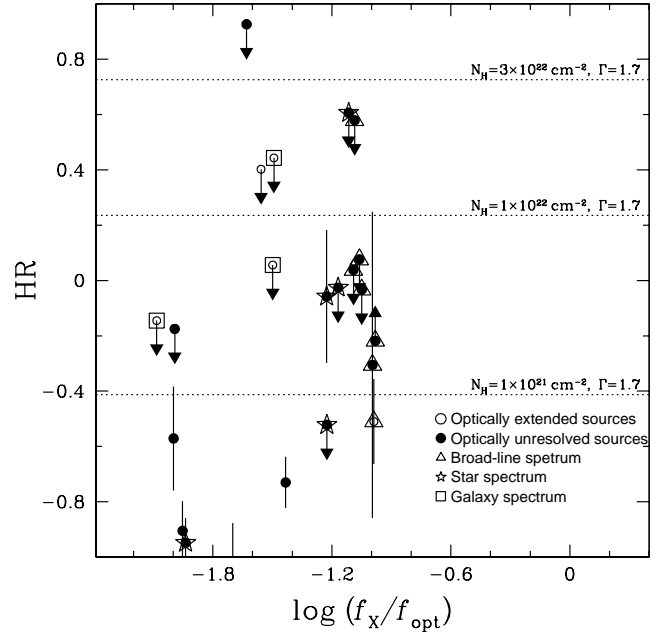


**Figure 4.** Hardness ratio against X-ray-to-optical flux ratio as defined in section 7 (eq. 3). The symbols are the same as in Figure 3. Upper and lower limits are for sources that are not detected in the hard and soft bands respectively to the EWAVELET detection threshold of  $5\sigma$ . In the case of soft/hard band non-detection a  $3\sigma$  upper limit to the count rate is estimated assuming Poisson statistics.

als/ellipticals at a mean redshift of  $z \approx 0.1$  by applying stacking methods. A statistically significant stacking signal was found for both the elliptical and the spiral galaxy sub-samples providing an estimate of the mean X-ray flux of these systems. We plot the surface density of the spiral galaxy sample used by Georgakakis et al. (2003a) at the mean X-ray flux of these systems estimated via stacking. This point is lower limit since it represents only a subset of the ‘normal’ galaxy population at the given flux limit.

The fluctuation analysis results of Miyaji & Griffiths (2002) are shown in Figure 5. The  $\log N - \log S$  constraints of these authors refer to the whole X-ray population (e.g. including AGNs) and not just the ‘normal’ galaxy sub-sample. Nevertheless, it has been suggested that ‘normal’ galaxies are likely to outnumber AGNs at faint fluxes (Hornschemeier et al. 2003) and therefore the Miyaji & Griffiths (2002) results are likely to be relevant to ‘normal’ galaxies at faint fluxes. In any case, the constraints provided by these authors are an upper limit to the ‘normal’ galaxy counts.

The model  $\log N - \log S$  prediction using the X-ray luminosity function derived by Georgantopoulos, Basilakos & Plionis (1999) for HII galaxies is also plotted in Figure 5. These authors convolved the local optical luminosity function of the Ho, Filippenko & Sargent (1995) sample with the corresponding  $L_X - L_B$  relation based on *Einstein* data to derive the X-ray luminosity function of different galaxy types. The galaxy classification scheme of the Ho et al. (1995) sample is highly reliable since it is based on high S/N nuclear optical spectra (Ho et al. 1997). Different X-ray luminosity evolution scenarios of the form

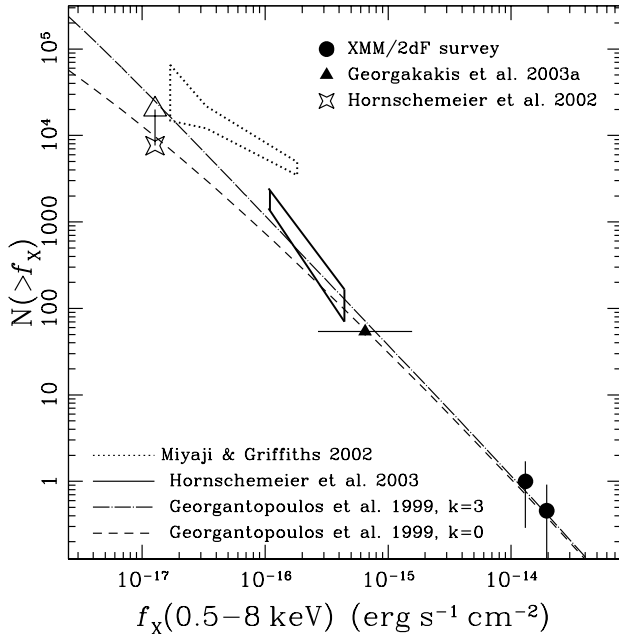


**Figure 5.** Cumulative ‘normal’ galaxy counts. Filled circles are the ‘normal’ galaxy candidates in the present study. The triangle represents the constraints from the stacking analysis results of Georgakakis et al. (2003a). The solid lined rectangle marks the region occupied by the source counts of Hornschemeier et al. (2003). The star is an upper limit to  $\log N - \log S$  from the stacking analysis results of Hornschemeier et al. (2002). The model predictions of the Georgantopoulos et al. (1999) X-ray luminosity function of H II galaxies assuming no evolution (dashed line) and luminosity evolution of the form  $L_X \sim (1+z)^3$  respectively (dot-dashed line) are also plotted. The dotted line is the fluctuation analysis constraints of Miyaji & Giffiths (2002) and should be regarded as an upper limit to the ‘normal’ galaxy counts.

$L_X \sim (1+z)^k$  are plotted. The difference between these two models at the flux range plotted here is small because the predicted mean redshift of star-forming galaxies at the flux limit  $f(0.5-8 \text{ keV}) \approx 10^{-16} \text{ erg s}^{-1} \text{ cm}^{-2}$  remains low. This is in agreement with the mean redshift of  $\approx 0.3$  of the Hornschemeier et al. (2003) deep ‘normal’ galaxy sample.

The  $k = 3$  evolutionary model is in fair agreement with both the Hornschemeier et al. (2003) and our  $\log N - \log S$  estimates. Although the Georgantopoulos et al. (1999) model is flatter (slope =  $-1.5$ ) than the Hornschemeier et al. (2003)  $\log N - \log S$  (slope =  $-1.74^{+0.28}_{-0.30}$ ), within the  $1\sigma$  uncertainties there is fair agreement. Also, the  $k = 3$  model is in better agreement with the Hornschemeier et al. (2003) observations over a wider flux range compared to the  $k = 0$  model. Although the difference between the two models is marginal in the flux range covered by the Hornschemeier et al. (2003) data the evidence above provides weak evidence for X-ray evolution of star-forming systems. As already discussed the mean redshift of ‘normal’ galaxies at the flux limits probed by Hornschemeier et al. (2003) is low and therefore any evolutionary effects are expected to be small. Deeper X-ray observations are required to detect ‘normal’ galaxies at moderate and high redshifts to better constrain their evolution.

## 9 CONCLUSIONS

In this paper we employ a wide field ( $2.5 \text{ deg}^2$ ) shallow ( $f_X(0.5-8 \text{ keV}) \approx 10^{-14} \text{ erg s}^{-1}$ ) XMM-Newton survey to investigate the nature of low X-ray-to-optical flux ratio sources,  $\log f_X/f_{opt} < -0.9$ . Our sample comprises 26 objects of which 20 have optical spectroscopic information. The majority of the sources without spectroscopic information have X-ray/optical properties that strongly suggest Galactic stars. Most of the spectroscopically identified systems are Galactic stars (total of 8) and broad line AGNs (total of 8).

We also find four sources with narrow emission and/or absorption line optical spectra. Two of them have X-ray/optical properties suggesting LLAGN activity. The remaining two sources have narrow emission line optical spectra, X-ray luminosities  $L_X \approx 10^{41} \text{ erg s}^{-1}$  and X-ray-to-optical flux ratios  $\approx -2$  suggesting ‘normal’ galaxies powered by star-formation activity.

The small number of ‘normal’ galaxies found in our wide field XMM/2dF survey is in agreement with the results from the 1 Ms ROSAT HRI survey of the Lockman Hole. Despite the poor statistics the estimated number density of ‘normal’ galaxies at the flux limit probed here is consistent with the  $\log N/\log S$  of deeper *Chandra* surveys extrapolated to bright fluxes. Using the X-ray luminosity function of local star-forming galaxies we find that the predicted  $\log N - \log S$  is in fair agreement with both our shallow and the deeper *Chandra* samples. The pure luminosity evolution model is in better agreement with the observations compared to the no-evolution prediction providing some evidence for X-ray evolution of star-forming spirals. However, the difference between the two models even at the flux limits of the 2 Ms *Chandra* Deep Field North survey is small and does not allow firm conclusions to be drawn. This is because of the low mean redshift ( $z \approx 0.3$ ) of the ‘normal’ galaxies probed by this ultra deep survey.

## 10 ACKNOWLEDGMENTS

We thank the anonymous referee for valuable comments and suggestions. This work is jointly funded by the European Union and the Greek Government in the framework of the programme ‘Promotion of Excellence in Technological Development and Research’, project ‘X-ray Astrophysics with ESA’s mission XMM’.

We acknowledge use of the 100k data release of the 2dF Galaxy Redshift Survey. The 2dF QSO Redshift Survey (2QZ) was compiled by the 2QZ survey team from observations made with the 2-degree Field on the Anglo-Australian Telescope.

Funding for the creation and distribution of the SDSS Archive has been provided by the Alfred P. Sloan Foundation, the Participating Institutions, the National Aeronautics and Space Administration, the National Science Foundation, the U.S. Department of Energy, the Japanese Monbukagakusho, and the Max Planck Society. The SDSS Web site is <http://www.sdss.org/>. The SDSS is managed by the Astrophysical Research Consortium (ARC) for the Participating Institutions. The Participating Institutions are The University of Chicago, Fermilab, the Institute for Advanced Study, the Japan Participation Group, The Johns Hop-

kings University, Los Alamos National Laboratory, the Max-Planck-Institute for Astronomy (MPIA), the Max-Planck-Institute for Astrophysics (MPA), New Mexico State University, University of Pittsburgh, Princeton University, the United States Naval Observatory, and the University of Washington.

## APPENDIX A: NOTES ON SELECTED SOURCES

**TGN 336Z130:** The X-ray centroid lies  $\approx 7$  arcsec away from the position of the optical galaxy. The probability of chance coincidence is small  $P = 0.6\%$ . Also, inspection of the X-ray centroid overlaid on the SDSS optical image in Figure 1 provides additional evidence that TGN 336Z130 is likely to be the correct counterpart of the X-ray source. In what follows we assume that TGN 336Z130 is the correct identification. The 2dFGRS optical spectrum of this  $B = 17.6$  mag systems exhibits absorption lines only suggesting an early type galaxy, most likely an E/S0. The X-ray-to-optical flux ratio of  $\approx -1.5$  and the X-ray luminosity  $L_X(0.5 - 8 \text{ keV}) \approx 8 \times 10^{41} \text{ erg s}^{-1}$  are consistent with those of ‘normal’ ellipticals with X-ray emission due to a hot gaseous halo. The hardness ratio upper limit ( $\text{HR} < 0.05$ ) indicates moderate photoelectric absorption  $\lesssim 6 \times 10^{21} \text{ cm}^{-2}$  ( $\Gamma = 1.7$ ). We note that the optical and X-ray properties of this source are reminiscent to those of X-ray bright optically inactive galaxies (Griffiths et al. 1995; Fiore et al. 2000; Comastri et al. 2002). Apart from the presence hot interstellar medium, other scenarios for the origin of the X-ray emission of TGN 336Z130 include (i) hot gas from a galaxy group, (ii) radiatively inefficient Advection Dominated Accretion Flow (ADAF), (iii) a LINER and (iv) a heavily obscured AGN. The X-ray source associated with TGN 336Z130 is not extended excluding the possibility of group emission. An ADAF or a LINER with the expected optical emission lines diluted by the host galaxy stellar light can explain the observed X-ray emission. This is particularly true in the case of spectra obtained through wide slits/fibres (like 2dF) that are contaminated by non-nuclear emission from the host galaxy (e.g. Ho, Filippenko & Sargent 1997; Moran et al. 2002; Severgnini et al. 2003). Comastri et al. (2002) in their multiwavelength study of FIORE-P3, the prototype of X-ray bright optically inactive systems, favor the heavily obscured Compton thick AGN scenario with the observed X-ray emission arising from a scattered nuclear component. However, for TGN 336Z130 this possibility is inconsistent with the observed soft X-ray spectral properties of this sources. We adopt a conservative approach and classify TGN 336Z130 an AGN. The low X-ray luminosity suggests a LLAGN. We note however, that this may also be a ‘normal’ galaxy with the X-ray emission arising from the hot interstellar medium.

**TGN 336Z208:** The optical counterpart of this X-ray source has extended optical light profile. Inspection of the SDSS image in Figure 1 suggests spiral galaxy morphology. The 2dFGRS spectrum reveals a broad-line AGN at  $z = 0.0736$ . The X-ray luminosity of this source  $L_X(0.5 - 8) = 1.8 \times 10^{42} \text{ erg s}^{-1}$  although elevated compared to ‘normal’ galaxies is lower than that of distant QSOs. The X-ray-to-optical flux ratio of  $\approx -1$  place this galaxy in the borderline between AGNs and ‘normal’ galaxies. The estimated

hardness ratio,  $\text{HR} = -0.51 \pm 0.15$ , suggests a soft X-ray spectrum consistent with the observed broad optical lines.

**TGN 336Z232:** The 2dFGRS optical spectrum of this system suggest an early type spiral with both emission ( $\text{H}\alpha$ ,  $[\text{N II}] 6583\text{\AA}$ ,  $[\text{O II}] 3727\text{\AA}$ ) and absorption ( $\text{H}+\text{K}$ ,  $\text{H}\beta$ ,  $\text{H}\gamma$ ,  $\text{H}\delta$ ,  $\text{NaD } 5893\text{\AA}$ ) lines. For the  $[\text{O II}] 3727\text{\AA}$  and the  $\text{H}\delta$  lines we estimate equivalent widths of the  $\text{EW}_{[\text{O II}]} \approx 12$  (emission) and  $\text{EW}_{\text{H}\delta} \approx -8\text{\AA}$  (absorption) respectively. On the basis of the Dressler et al. (1999) classification scheme TGN 336Z232 is e(a) type galaxy. Poggianti et al. (1999) discuss that the optical spectral properties of this class of galaxies can be explained by a starburst event followed by a period of much low star-formation activity. They also argue that in the local Universe e(a) type galaxies are frequently associated with dusty interacting/merging systems. Assuming that the  $[\text{O II}] 3727\text{\AA}$  line of TGN 336Z232 is due to star-formation, the observed X-ray emission may arise from a starburst event in the recent past. The X-ray-to-optical flux ratio of  $-1.5$  and the X-ray luminosity,  $L_X(0.5 - 8) \approx 8 \times 10^{41} \text{ erg s}^{-1}$ , cannot discriminate between an AGN or X-ray properties dominated by stellar processes. The hardness ratio  $3\sigma$  upper limit ( $\text{HR} < 0.44$ ) corresponds to photoelectric absorption  $\lesssim 1.5 \times 10^{22} \text{ cm}^{-2}$  ( $\Gamma = 1.7$ ) and cannot strongly constrain the X-ray spectral properties or the nature of this source. We adopt a conservative approach and classify this source an AGN. The low X-ray luminosity suggest LLAGN.

**UM 603:** This narrow emission line galaxy is classified as H II on the basis of its optical spectral properties (Terlevich et al. 1991). Its X-ray luminosity  $L_X(0.5 - 8) = 1.5 \times 10^{41} \text{ erg s}^{-1}$  and X-ray-to-optical flux ratio  $\approx -2.1$  also suggest ‘normal’ galaxy. Moreover, this source is not detected in the hard-band suggesting a soft X-ray spectrum,  $\text{HR} < -0.14$ , consistent with stellar origin of the X-ray emission.

**TGN 336Z243:** In the SDSS optical image this galaxy appears to be interacting with a nearby smaller system. The X-ray centroid is offset by 3 arcsec from the optical centre of the galaxy. This is a narrow emission line system at  $z = 0.0717$  showing  $[\text{O III}] 4959 + 5007\text{\AA}$  doublet,  $\text{H}\alpha$  and  $[\text{N II}] 6583 \text{\AA}$ . Although the signal-to-noise ratio of the spectrum is low,  $\text{H}\beta$  is not visible in emission. This coupled with the strong  $[\text{O III}] 5007\text{\AA}$  feature may suggest a Seyfert 2 type system. A hardness ratio has not been estimated for this source because it is not detected in either the 0.5-2 keV or the 2-8 keV images to the formal EWAVELET detection threshold of  $5\sigma$ . Moreover, the low X-ray luminosity  $L_X(0.5 - 8) = 1.9 \times 10^{41} \text{ erg s}^{-1}$  and X-ray-to-optical flux ratio  $\approx -2.0$  are consistent with a ‘normal’ galaxy powered by stellar processes.

**B005615.26-275548.8:** The X-ray centroid lies 5 arcsec off the optical source centre. The probability of chance coincidence is 1.5%. The counterpart of the X-ray source (assuming it is the correct one) is optically extended and has no optical spectroscopic information. The optical-to-X-ray flux ratio of  $\approx -1.6$  place this source in the ‘normal’ galaxy regime. The hardness ratio upper limit ( $\text{HR} < 0.40$ ) indicates photoelectric absorption  $\lesssim 1.5 \times 10^{22} \text{ cm}^{-2}$  ( $\Gamma = 1.7$ ) and cannot strongly constrain the X-ray spectral properties or the nature of this source. On the basis of the above evidence alone we cannot conclude on the nature of this source.

**Other sources:** A number sources (ID numbers in Table 1: #3, 12, 20, 23, 26) in the present sample (have no optical spectral information. However, they share common properties: unresolved optical light profile, soft X-ray spectra and low X-ray-to-optical flux ratio that strongly suggest Galactic stars. Sources in the North Galactic Pole region (#3, #12) also have colour information from the SDSS. Source #3 however, is too bright ( $B \approx 13.5$  mag) and saturated on the SDSS images. This does not allow meaningful colours to be estimated. Source #12 has  $g-r$ ,  $u-g$  colours of 0.5 and 1.5 respectively, typical of stellar colours (e.g. Stoughton et al. 2002, their Fig. 13).

## REFERENCES

- Alexander D. M., Aussel H., Bauer F. E., Brandt W. N., Hornschemeier A. E., Vignali C., Garmire G. P., Schneider D. P., 2002, *ApJ*, 568, L85.
- Barger A. J., Cowie L. L., Brandt W. N., Capak P., Garmire G. P., Hornschemeier A. E., Steffen A. T., Wehner E. H., 2002, *AJ*, 124, 1839.
- Bauer F. E., Alexander D. M., Brandt W. N., Hornschemeier A. E., Vignali C., Garmire G. P., Schneider D. P., 2002, *AJ*, 124, 2351
- Bertin E., Arnouts S., 1996, *A&AS*, 117, 393
- Brandt W. N., Hornschemeier A. E., Schneider D. P., Alexander D. M., Bauer F. E., Garmire G. P., Vignali C., 2001a, *ApJ*, 558, 5.
- Brandt W. N., Hornschemeier A. E., Alexander D. M., Garmire G. P., Schneider D. P., Broos P. S., Townsley L. K., Bautz M. W., Feigelson E. D., Griffiths R. E., 2001b, *AJ*, 122, 1.
- Brandt W. N., 2001c, *AJ*, 122, 2810.
- Croom S. M., Smith R. J., Boyle B. J., Shanks T., Loaring N. S., Miller L., Lewis I. J., 2001, *MNRAS*, 322L, 29
- Colless M., Dalton G., Maddox S. et al., 2001, *MNRAS*, 328, 1039.
- Comastri A., et al. 2002, *ApJ*, 571, 771.
- Downes A. J. B., Peacock J. A., Savage A., Carrie D. R., 1986, *MNRAS*, 218, 31
- Dressler A., Smail I., Poggianti B. M., Butcher H., Couch W. J., Ellis R. S., Oemler A. Jr., 1999, *ApJS*, 122, 51
- Elvis M., Soltan A., Keel W., 1984, *ApJ*, 283, 479
- Fiore F., La Franca F., Vignali C., Comastri A., Matt G., Perola G. C., Cappi M., Elvis M., Nicastro F., 2000, *NewA*, 5, 143
- Fukugita M., Ichikawa T., Gunn J. E., Doi M., Shimasaku K., Schneider D. P., 1996, *AJ*, 111, 1748
- Georgakakis A., Georgantopoulos I., Stewart G. C., Shanks T., Boyle B. J., 2003a, *MNRAS*, in press, astro-ph/0305278
- Georgakakis A., Hopkins A. M., Sullivan M., Afonso J., Georgantopoulos I., Mobasher B., Cram L. E., 2003b, *MNRAS*, submitted
- Georgantopoulos I., Basilakos S., Plionis M., 1999, *MNRAS*, 305, L31.
- Georgantopoulos I., Stewart G. C., Shanks T., Boyle B. J., Griffiths R. E., 1996, *MNRAS*, 280, 276.
- Griffiths R. E., Georgantopoulos I., Boyle B. J., Stewart G. C., Shanks T., Della Ceca R., 1995, *MNRAS*, 275, 77.
- Griffiths R. E., Della Ceca R., Georgantopoulos I., Boyle B. J., Stewart G. C., Shanks T., Fruscione A., 1996, *MNRAS*, 281, 71.
- Hasinger G., Altieri B., Arnaud, M. et al., 2001, *A&A*, 365, L45.
- Ho L. C., Filippenko A. V., Sargent W., 1995, *ApJS*, 98, 477.
- Ho L. C., Filippenko A. V., Sargent W., 1997, *ApJS*, 112, 315.
- Hornschemeier A. E., Brandt W. N., Alexander D. M., Bauer F. E., Garmire G. P., Schneider D. P., Bautz M. W., Chartas G., 2002a, *ApJ*, 568, 82.
- Hornschemeier A. E., Bauer F. E., Alexander D. M., Brandt W. N., Sargent W. L. W., Vignali C., Garmire G. P., Schneider D. P., 2003, *AJ*, accepted, astro-ph/0305086.
- Kim D. W., Fabbiano G., Trinchieri G., 1992, *ApJ*, 393, 134.
- Landolt A. U., 1992, *AJ*, 104, 340
- Lehmann I., et al., 2001, *A&A*, 371, 833.
- Lilly S. J., Le Fevre O., Hammer F., Crampton D., 1996, *ApJ*, 460, L1.
- Maddox S. J., Sutherland W. J., Efstathiou G., Loveday J., Peterson B. A., 1990, *MNRAS*, 247L, 1
- McHardy I. M., et al., 1998, *MNRAS*, 295, 641
- McHardy I. M., Gunn K. F., Newsam A. M., Mason K. O., Page M. J., Takata T., Sekiguchi K., Sasseeen T., Cordova F., Jones L. R., Loaring N., 2003, *MNRAS*, in press, astro-ph/0302553
- Metcalfe N., Fong R., Shanks T., 1995, *MNRAS*, 274, 769
- Miyaji T., Griffiths R. E., 2002, *ApJ*, 564L, 5
- Moran E. C., Lehnert M. D., Helfand D. J., 1999, *ApJ*, 526, 649
- Moran E., Filippenko A. V., Chornock R., 2002, *ApJ*, 579L, 71
- O’Sullivan E., Forbes D. A., Ponman T. J., 2001, *MNRAS*, 328, 461.
- Poggianti B. M., Smail I., Dressler A., Couch W. J., Barger A. J., Butcher H., Ellis R. S., Oemler A. Jr., 1999, *ApJ*, 518, 576
- Roche N., Griffiths R. E., Della Ceca R., Shanks T., Boyle B. J., Georgantopoulos I., Stewart G. C., 1996, *MNRAS*, 282, 820
- Severgnini P. et al., 2003, *A&A*, 406, 483
- Stocke J. T., Morris S. L., Gioia I. M., Maccacaro T., Schild R., Wolter A., Fleming T. A., Henry J. P., 1991, *ApJS*, 76, 813
- Stoughton C., et al., 2002, *AJ*, 123, 485.
- Strüder L., Briel U., Dennerl K., et al. 2001, *A&A*, 365, L18.
- Turner M. J. L., Abbey A., Arnaud M., et al., 2001, *A&A*, 365, L27.
- York D. G., et al., 2000, *AJ*, 120, 1579.